

Article

# Effect of Different Carbon Supports on the Activity of PtNi Bimetallic Catalysts toward the Oxygen Reduction

Juan C. Ortíz-Herrera <sup>1</sup>, Miriam M. Tellez-Cruz <sup>2</sup> , Omar Solorza-Feria <sup>3</sup>  and Dora I. Medina <sup>1,\*</sup> 

<sup>1</sup> Tecnológico de Monterrey, School of Engineering and Sciences, Atizapan de Zaragoza 52926, Estado de Mexico, Mexico; devox@live.com.mx

<sup>2</sup> Tecnológico Nacional de México, Instituto Tecnológico del Valle de Etna, Abasolo S/N, Barrio del Agua Buena, Santiago Suchilquitongo, Oaxaca 68230, Guerrero, Mexico; miriam.tc@itvalletla.edu.mx

<sup>3</sup> Departamento de Química, Cinvestav, Av. Instituto Politécnico Nacional 2508, San Pedro Zacatenco, Gustavo A. Madero, Ciudad de Mexico 07360, Mexico; osolorza@cinvestav.mx

\* Correspondence: dora.medina@tec.mx

**Abstract:** To evaluate supports' effects on catalytic activity toward the oxygen reduction reaction (ORR), a simple and controlled chemical synthesis, involving the hot injection of metal precursors, was developed to produce bimetallic PtNi nanoparticles (75 wt.% Pt and 25 wt.% Ni), supported on carbon nanotubes (CNTs) and carbon nanofibers (CNFs). The synthesized electrocatalyst was characterized using X-ray diffraction (XRD), energy dispersive X-ray spectroscopy (EDS), and scanning transmission electron microscopy (STEM). To determine the catalytic activity, an electrochemical evaluation of the synthesized catalysts in an acidic medium was performed using cyclic voltammetry (CV), CO stripping, and rotating disk electrode (RDE) tests. The presence of Pt and Ni in the nanoparticles was confirmed by EDS and XRD. Based on the STEM micrographs, the average particle size was 30 nm. Compared to the commercial Pt/C catalyst, the PtNi/CNT catalyst exhibited higher specific activity and slightly lower mass activity toward ORR in a 0.1 M HClO<sub>4</sub> electrolyte solution.

**Keywords:** polymer electrolyte membrane fuel cell; oxygen reduction reaction; carbon nanotubes; carbon nanofibers; electrocatalysts



**Citation:** Ortíz-Herrera, J.C.; Tellez-Cruz, M.M.; Solorza-Feria, O.; Medina, D.I. Effect of Different Carbon Supports on the Activity of PtNi Bimetallic Catalysts toward the Oxygen Reduction. *Catalysts* **2022**, *12*, 477. <https://doi.org/10.3390/catal12050477>

Academic Editors: Alexander D. Modestov and Serguei A. Martémianov

Received: 11 March 2022

Accepted: 20 April 2022

Published: 23 April 2022

**Publisher's Note:** MDPI stays neutral with regard to jurisdictional claims in published maps and institutional affiliations.



**Copyright:** © 2022 by the authors. Licensee MDPI, Basel, Switzerland. This article is an open access article distributed under the terms and conditions of the Creative Commons Attribution (CC BY) license (<https://creativecommons.org/licenses/by/4.0/>).

## 1. Introduction

Polymer electrolyte membrane fuel cells (PEMFCs) are a promising alternative clean energy source for fixed and stationary applications. However, to promote its commercialization, several of the major challenges that this technology raises must be overcome, such as the sluggish kinetics of the oxygen reduction reaction (ORR), lack of long-term catalyst stability, and the high cost of platinum [1,2]. In this regard, developing catalysts that are Pt-free or have a low Pt content while maintaining catalytic activity is critical. One option for achieving these objectives is to reduce the Pt loading when developing catalysts made of Pt-alloys and other metals, such as Ni, Co, Fe, or other elements [3–5]. For example, some studies have shown that catalysts made from bimetallic alloys with Pt exhibit catalytic activity similar to, or higher than, carbon-supported Pt (Pt/C) catalysts [6–8]. In the last few years, different approaches for improving the catalytic activity of Pt bimetallic alloy catalysts have been developed by modifying the shapes, compositions, or sizes of the nanoparticles [9].

On the other hand, the exploration of carbon-based support materials remains of vital importance in order to provide greater stability of catalysts and the durability of fuel cells, therefore maintaining optimal performance for a longer time. Similarly, the research of carbon-based support materials becomes crucial for improving the stability and durability of catalysts to maintain optimal performance for a long time. Carbon-based materials, such as carbon black, are the most commonly used support materials, but some carbon allotropes are also good choices due to their structure and attractive properties. Carbon nanotubes

(CNTs) and carbon nanofibers (CNFs) are two examples of these supports [10–14]. CNTs have a stronger corrosion resistance in acidic media than carbon black, which is one of their advantages. In this type of catalyst, the stability of the carbon supports may affect the loss of the Pt surface area due to the agglomeration and detachment of Pt-based nanoparticles [15]. CNFs have also been used as catalyst support materials in fuel cells [16]. The main difference between CNTs and CNFs is that CNFs, in contrast to CNTs, have a very thin hollow cavity or no hollow cavity. In addition, CNFs have a much larger diameter than CNTs [17]. To facilitate gas adsorption and optimize the use of pristine CNTs and pristine CNFs as catalyst support materials for cathodic reaction, their surfaces must be modified [18,19]. Different methods that are used to deposit nanoparticles on carbon black, such as impregnation [20,21], ultrasound [22], precipitation [23], and others, have also been used for nanoparticle deposition on pristine CNTs and pristine CNFs [17].

Regarding the research of PtNi bimetallic electrocatalysts for the ORR, we proposed a strategy for the design, synthesis, and characterization of a PtNi bimetallic electrocatalyst supported on carbon-based materials. The electrocatalyst with the best catalytic activity exhibited a higher specific activity and a slightly lower mass activity for the ORR in acid medium. It is important to mention some of the precedents that serve as a starting point for this PtNi system and the carbon supports [24–31]. In this regard, Asset et al. studied different properties that influence the catalytic activity of the catalysts due to the support material. In this study, three different types of carbon blacks, graphene nanosheets, carbon xerogel, and CNT, were used. They showed higher specific activity and mass activity values for the PtNi/XC72 catalyst compared to the PtNi/CNT catalyst [24]. On the other hand, Du et al. reported a simple one-pot synthesis of a PtNi-MWCNT hybrid structure. The PtNi-MWCNT catalyst presented an almost double mass activity and a higher specific activity compared to the Pt/C catalyst [25].

Although there are some studies on the effect of the structure of different carbon supports on the catalytic activity of the PtNi [24–31] alloy, as far as the authors' knowledge, there are no studies comparing the effect of materials, such as pristine carbon nanofibers, pristine carbon nanotubes, and commercial carbon black.

This study is focused on obtaining PtNi nanoparticles through a versatile synthesis and the evaluation of the effect of supports on the catalytic activity of PtNi nanoparticles, which are supported on pristine CNTs and pristine CNFs towards oxygen reduction in acid medium, since existing studies in the literature consider only Pt nanoparticles or Pt alloys with some other metal and CNFs with some type of surface modification as support for ORR catalysts, compared to CNTs.

In this work, the synthesis, physical characterization, and electrochemical evaluation of the PtNi bimetallic electrocatalyst supported on pristine carbon materials are investigated. PtNi catalysts were produced with a simple and low-cost chemical synthesis with oleylamine, which has demonstrated to be a versatile method to produce Pt<sub>3</sub>Ni/C bimetallic nanocatalysts with controlled size, composition, and shape. Hence, we have adjusted these protocols [32,33] to synthesize PtNi bimetallic nanoparticles supported on pristine carbon materials to obtain electrocatalysts for the ORR.

The main objective of this work is to evaluate the effect of different carbon supports on the activity of catalysts for oxygen reduction, obtaining bimetallic PtNi nanoparticles through a reproducible synthesis with the use of oleylamine and a hot injection of the metal precursors and the support of nanoparticles obtained with pristine CNTs or pristine CNFs without any previous treatment to determine how the supports affect the catalytic activity in the electrocatalysts obtained. Herein, we describe the synthesis of bimetallic PtNi nanoparticles (75 wt.% Pt and 25 wt.% Ni). Oleylamine was used as a solvent, surfactant, and mild reducing agent. This synthesis method has proven to be effective in producing nanoparticles with controlled composition, size, shape, and crystalline structure [34]. This synthesis method has certain advantages since it does not require a mixture of solvents as reducing agents, nor treatment of the metal precursors or any additional purification process of reagents used [35]. The bimetallic nanoparticles were characterized using X-

ray diffraction (XRD), energy dispersive X-ray (EDS), and scanning transmission electron microscopy (STEM). Finally, the ORR activity of the nanoparticles was investigated by performing cyclic voltammetry (CV), CO stripping, and rotating disk electrode (RDE) tests in a 0.1 M HClO<sub>4</sub> electrolyte solution. The PtNi/CNT and PtNi/CNF catalysts' performances were compared to that of a commercial Pt/C catalyst.

## 2. Results and Discussion

### 2.1. Physical Characterization of the PtNi Nanoparticles

Figure 1 shows the XRD pattern of the PtNi nanoparticles that were synthesized using the oleylamine route. The XRD pattern of nonsupported PtNi nanoparticles is presented to better exhibit the crystalline phases of the synthesized material. The PtNi face-centered cubic (FCC) phase is represented by green bars below the experimental pattern, which is similar to the standard crystallographic tables (ICDD PDF-2: 03-065-9445). The Bragg reflections that appear at 41.28°, 48.04°, 70.29°, and 84.90° are associated with the (111), (200), (220), and (311) planes of the PtNi alloy. The diffraction pattern of PtNi differs slightly from the characteristic patterns of pure metals (Pt represented by orange bars and Ni by purple bars below the experimental patterns). The Pt (111) diffraction peak is slightly shifted, which could be due to the compression deformation of the Pt atom in the Ni FCC lattice during the formation of the PtNi alloy [36]. This result suggests that the two elements coexist in the synthesized nanoparticles, resulting in the formation of a bimetallic system. Moreover, in the synthesized nanoparticles, there are no peaks that are associated with the formation of nickel oxides or hydroxides. Figure 1 also shows the XRD patterns of the supported PtNi nanoparticles in the CNTs and CNFs, presenting the Bragg reflections of the XRD pattern of the unsupported PtNi nanoparticles associated with the corresponding planes mentioned above; the XRD patterns of the supported PtNi nanoparticles show an additional Bragg reflection at 25.71° and 26.48° for the CNTs and CNFs, respectively, associated with the representative peak corresponding to the plane (002) of the carbon material used as support.

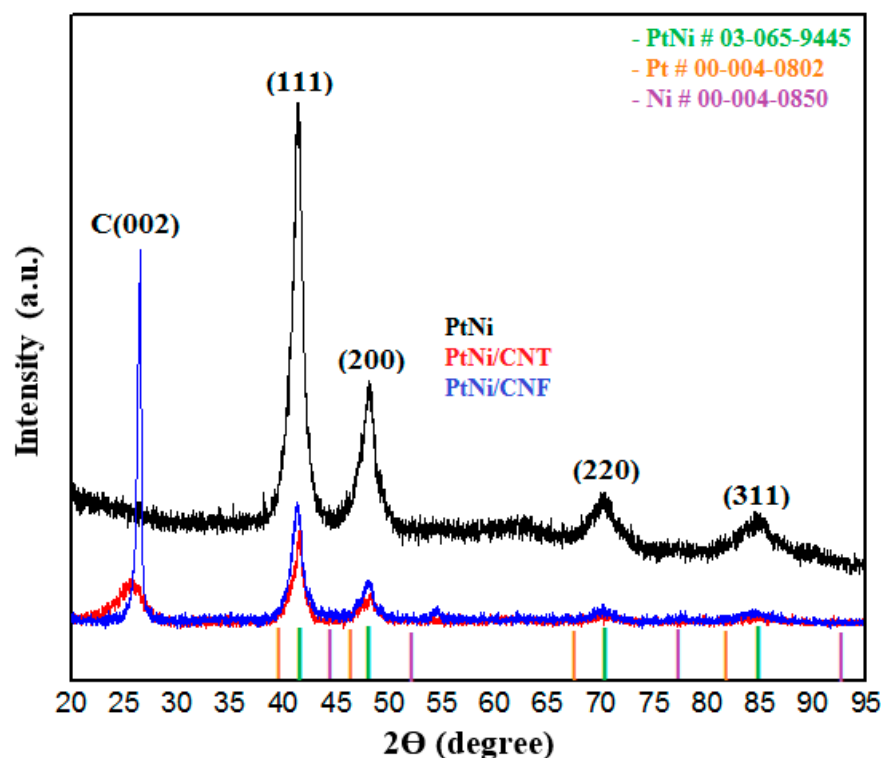
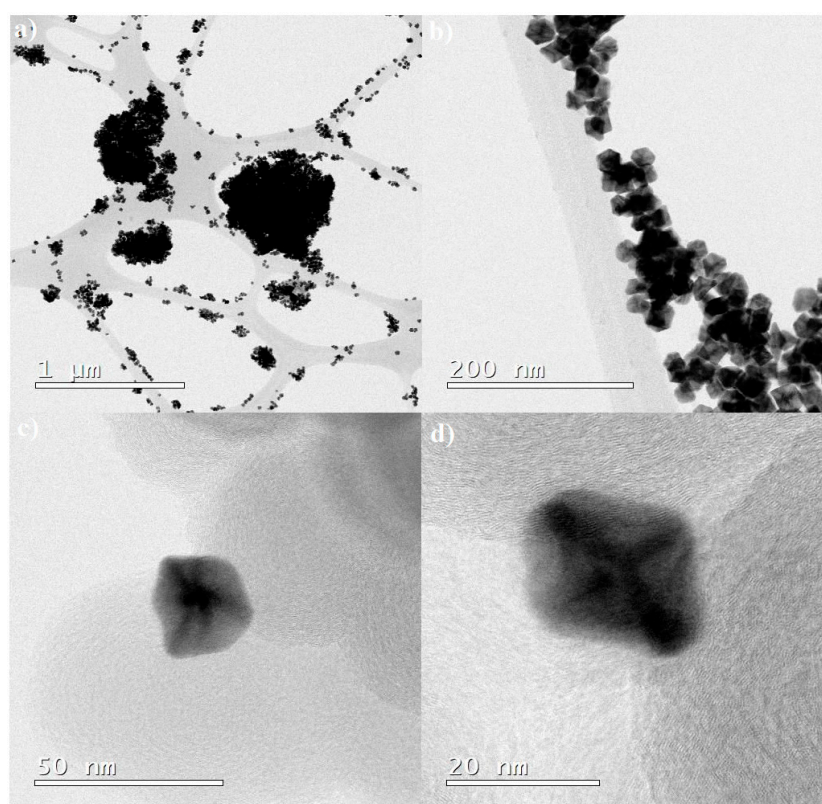


Figure 1. Powder diffraction patterns of the PtNi, PtNi/CNT and PtNi/CNF.

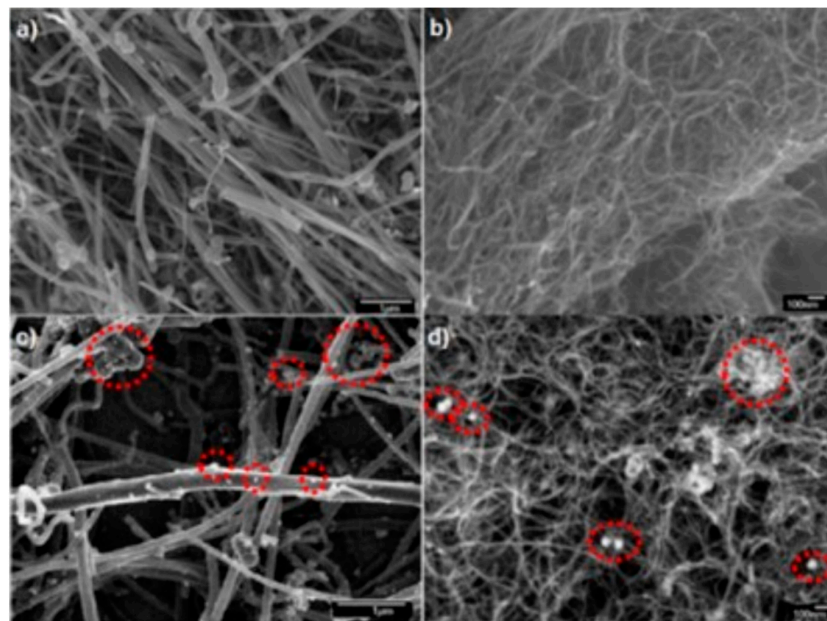
Figure 2 shows STEM images of the morphology and distribution of the as-synthesized nanoparticles. The PtNi nanoparticles have well-dispersed, uniform shapes and sizes on the carbon support, which is favorable for ORR since agglomeration decreases the catalytic activity of the cathodic reaction [37,38]. Figure 2a,b show the dispersion of the nanoparticles. Conversely, Figure 2c,d show representative morphologies of the synthesized nanoparticles and polyhedral nanoparticles with well-defined morphologies. According to the literature, nanoparticles with well-defined shapes, such as octahedrons, icosahedrons, and truncated octahedrons, have demonstrated better catalytic activity than commercial Pt/C nanoparticles [39]. The size and shape of nanoparticles play an important role in catalysis because they determine the active sites for the ORR [40]. This evidence suggests that the increase in the catalytic activity of the bimetallic PtNi nanoparticles, which were synthesized using this simple method, can be partially attributed to their well-defined morphologies. The obtained PtNi nanoparticles have an average size of 30 nm.



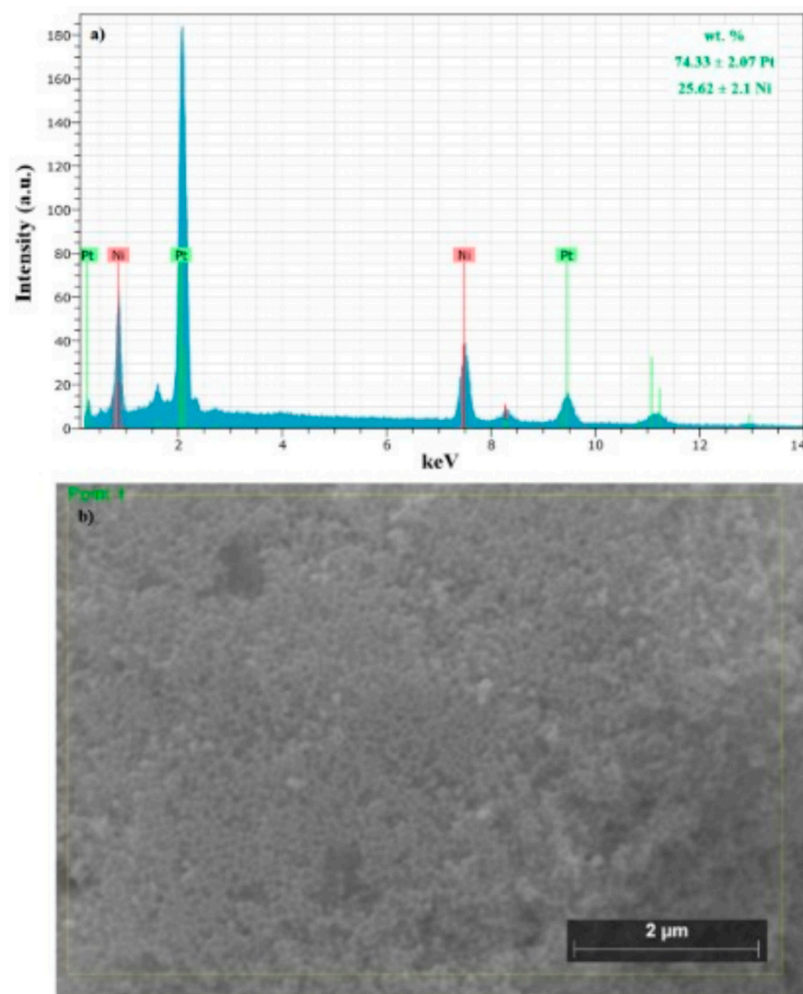
**Figure 2.** (a–d) STEM images of PtNi nanoparticles supported on Vulcan carbon.

Figure 3a,b show the micrographs of the as-received CNTs and CNFs used as support materials for the synthesized PtNi nanoparticles. Figure 3c,d show images of the PtNi nanoparticles supported on the CNTs and CNFs, respectively. It was demonstrated that the deposition method used for the PtNi nanoparticles on the proposed support materials was simple and effective.

Figure 4 also shows the EDS–SEM analysis results of the chemical composition of the PtNi/C nanoparticles. The presence of Pt and Ni was confirmed in the obtained spectrum of the nanoparticles. Additionally, EDS–SEM was performed using three different measurements of equal areas on the same sample to be as representative as possible. Figure 4b shows one of the areas determined to estimate the chemical composition of the PtNi nanoparticles. EDS–SEM was used in a semi-quantitative analysis to estimate the chemical composition of the nanoparticles. The measured compositions using EDS–SEM were  $74.33 \pm 2.07$  wt.% Pt and  $25.62 \pm 2.1$  wt.% Ni, which agree with the nominal compositions (75 wt.% Pt and 25 wt.% Ni).



**Figure 3.** SEM images (a) Carbon nanofibers (CNF), and (b) Carbon nanotubes (CNT). PtNi nanoparticles supported on (c) CNF and (d) CNT. Scale bars are 1 μm (a,c) and 100 nm (b,d). The red circles in the SEM image show the presence of the PtNi nanoparticles in the corresponding supports.



**Figure 4.** (a) EDS-SEM spectrum of Pt and Ni in the PtNi nanoparticles and (b) area analyzed to estimate the chemical composition of the PtNi nanoparticles.

## 2.2. Electrochemical Characterization of PtNi/CNT and PtNi/CNF

The electrocatalytic activity of the PtNi/CNT and PtNi/CNF electrocatalysts toward the ORR were evaluated in a typical three-electrode electrochemical cell using the electrochemical activity of the commercial Pt/C catalysts as a reference. Prior to polarization experiments, electrochemical activation was used to characterize and clean the freshly prepared electrode surface using a scanning potential range of 0.05–1.2 V vs. RHE in N<sub>2</sub>-purged 0.1 M HClO<sub>4</sub> to obtain a reproducible cyclic voltammogram. Figure 5 shows the voltammograms of the PtNi/CNT, PtNi/CNF, and Pt/C catalysts in acid media. Hydrogen adsorption–desorption peaks are observed in the potential range of 0.05–0.3 V vs. RHE, and the double-layer capacitance is observed in the potential range of 0.3–0.8 V vs. RHE. The adsorption of oxides and hydroxides in the catalytic material is observed in the anodic scan potential range of 0.8–1.2 V vs. RHE. When the synthesized materials' voltammograms were compared to that of Pt/C, slight differences were discovered in three regions (the hydrogen zone, the double-layer capacitance, and the oxide formation region). The cyclic voltammogram of the PtNi/CNT and PtNi/CNF catalysts shows a positive shift in current reduction peaks of the OH<sub>ads</sub> species adsorbed on the electrode surfaces compared to that of Pt. This behavior reflects the weakening of the adsorption energy of reactive intermediates [41]. In general, the low OH<sub>ads</sub> on the electrode surface correlated with the reported Pt profile in acid media [37,42].

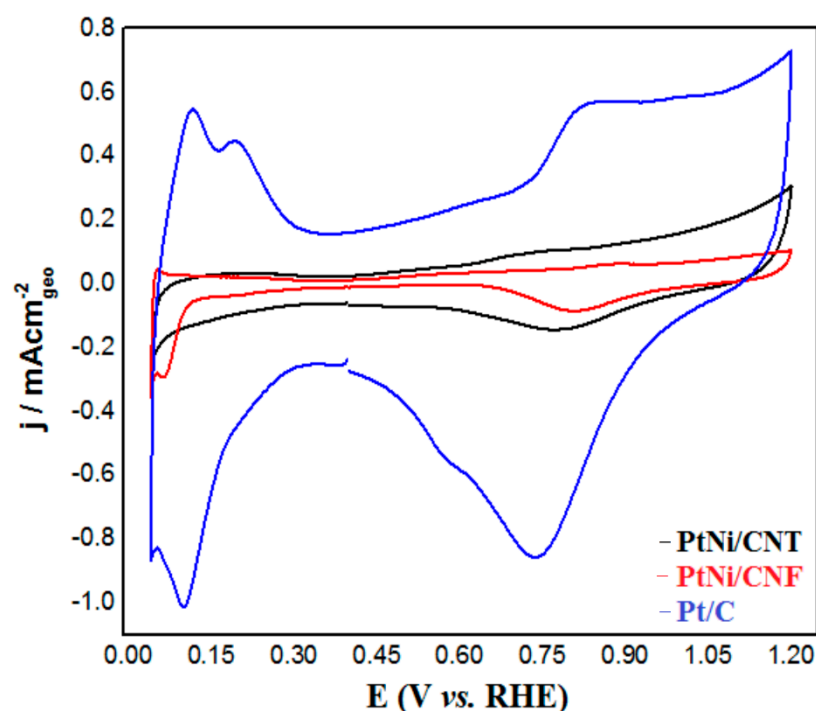


**Figure 5.** Cyclic voltammograms of the catalysts in 0.1 M HClO<sub>4</sub> (the black line represents PtNi/CNT, the red line represents PtNi/CNF, and the blue line represents Pt/C).

The electrochemical oxidation of adsorbed CO is generally used to determine the electrochemical active surface area (ECSA), which is an essential parameter in evaluating specific activity (SA) and comparing different catalysts for the ORR [43–45].

The ECSAs of the PtNi/CNT, PtNi/CNF, and Pt/C catalysts were determined using previously reported procedures of the CO stripping technique [46,47]. CO stripping on Pt nanoparticles usually shows peak multiplicity observed in the oxidation of an adsorbed CO layer. Figure 6 shows the CO-stripping peaks of the PtNi/CNT, PtNi/CNF, and Pt/C catalysts. The synthesized materials are observed to have peaks at smaller displacements compared to Pt/C; the PtNi/CNT and PtNi/CNF peaks appear to be centered in 0.74 and 0.70 V vs. RHE, whereas the Pt/C peak appears to be centered in 0.78 V vs. RHE. This

result is consistent with previous research that suggests that CNTs and CNFs are more CO tolerant than carbon black [10]. The peak potential of the Pt-based catalysts is closely related to the crystallographic planes exposed to the electrolyte and the shape/size of the nanoparticles [45]. In the CO peak, the broad peaks corresponding to the PtNi/CNT and PtNi/CNF catalysts differ from each other, and from those of the Pt/C catalysts, which could be due to different factors, such as crystalline surface defects (e.g., terraces and kinks) or surface defects created during the synthesis [48].

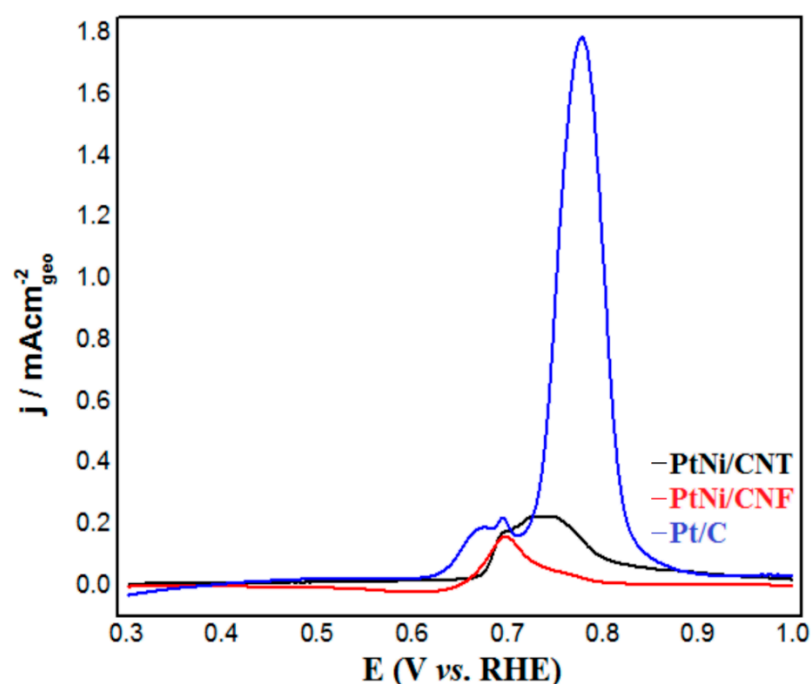


**Figure 6.** CO-stripping voltammetry curves of the catalysts in 0.1 M HClO<sub>4</sub>.

Table 1 presents the determined ECSA values of the PtNi/CNT, PtNi/CNF, and Pt/C catalysts. The results show that the PtNi/CNT and PtNi/CNF catalysts had lower ECSA values than the Pt/C catalysts. The low ECSA values of the PtNi/CNT and PtNi/CNF catalysts compared to those of Pt/C may have resulted because the CNTs and CNFs were used without any surface modification treatment in order to enhance the low reactivity exhibited by pristine CNTs and pristine CNFs. We also present the SA and MA results of other studies that reported the results for PtNi/CNT (the CNTs were modified), PtNi/C, and Pt/C [24,31] as a reference of other published studies.

**Table 1.** Kinetic parameters deduced from the ORR on PtNi/CNT, PtNi/CNF, PtNi/C and Pt/C catalysts in O<sub>2</sub>-saturated 0.1 M HClO<sub>4</sub>.

Catalysts	ECSA (m <sup>2</sup> g <sup>-1</sup> Pt)	SA @ 0.9 V (mA cm <sup>-2</sup> Pt)	MA @ 0.9 V (A mg <sup>-1</sup> Pt)	Tafel Slope (mV dec <sup>-1</sup> )	B <sub>0</sub> (mA cm <sup>-2</sup> rpm <sup>-1/2</sup> )
PtNi/CNT	12.15	1.45	0.18	84.9	0.1245
PtNi/CNF	6.72	1.47	0.10	79.8	0.1263
Pt/C	53.22	0.35	0.19	69.1	0.1080
PtNi/CNT <sup>a</sup> [24]	-	0.98	0.28	-	-
PtNi/C [24]	-	1.29	0.59	-	-
PtNi/CNT <sup>b</sup> [31]	-	1.38	0.48	-	-
Pt/C [31]	-	0.16	0.09	-	-

<sup>a</sup> and <sup>b</sup>: modified CNT.

The electrochemical RDE technique was used to study the kinetics of the ORR on the PtNi/CNT, PtNi/CNF, and Pt/C catalysts because of the strong dependence of the ORR on hydrodynamic conditions. Potentiodynamic tests were performed for the ORR at 25 °C in an O<sub>2</sub>-saturated 0.1 M HClO<sub>4</sub> electrolyte. Figure 7 shows sigmoidal polarization curves of the PtNi/CNT, PtNi/CNF, and Pt/C catalysts for the ORR obtained at 1600 rpm in a potential range of 0.05–1.05 V vs. RHE at 20 mV s<sup>-1</sup>. Three zones are distinguished for the tested materials: (1) the kinetic control (1.05–0.99 V vs. RHE), (2) the mixed kinetic-diffusion (0.99–0.65 V vs. RHE), and (3) mass transport (0.65–0.20 V vs. RHE). The PtNi/CNT, PtNi/CNF, and Pt/C catalysts had half-wave potentials ( $E_{1/2}$ ) of 0.89, 0.87, and 0.89 V vs. RHE, respectively. These results agree with those reported in the literature, and they indicate that our synthesized PtNi/CNT material could be used as a cathodic catalyst in PEMFCs. An increase in the limiting current density of the PtNi/CNT and PtNi/CNF catalysts was observed at high overpotentials between 0.65 and 0.20 V vs. RHE. The increase in the limiting current of the synthesized catalyst could be due to an increase in oxygen diffusion across the surface of the ink-type working electrode.

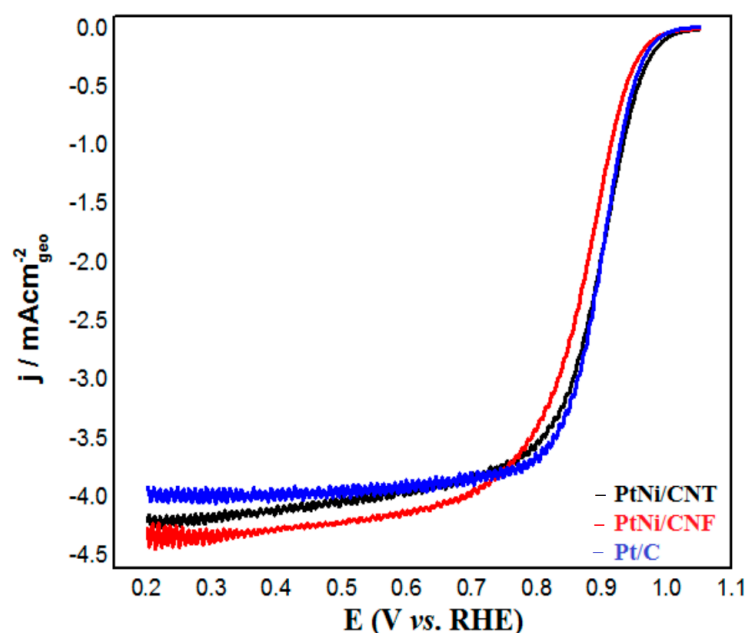


**Figure 7.** ORR polarization curves for the PtNi/CNT, PtNi/CNF and Pt/C catalysts in O<sub>2</sub>-saturated 0.1 mol L<sup>-1</sup> HClO<sub>4</sub> solution at a scan rate of 20 mV s<sup>-1</sup> and rotation rate of 1600 rpm.

Kinetic analyses were performed for the SA and mass activity (MA) calculations. The procedures for the kinetic current corrections, SA measurement, and MA measurement were conducted according to a previously described protocol [47]. The catalytic activities of the catalysts were investigated using Tafel plot values. Figure 8 shows mass-transfer-corrected Tafel plots of the PtNi/CNT and PtNi/CNF catalysts, with Tafel slopes of 84.9 and 79.8 mV dec<sup>-1</sup>, respectively. These slope values are higher than that of the Pt/C catalyst (69.1 mV dec<sup>-1</sup>). The Tafel slope values for all the synthesized bimetallic catalysts indicate fast ORR kinetics due to the formation of the PtNi alloy in the catalyst. Table 1 shows the calculated SA and MA values. As can be observed, the MA value of the PtNi/CNT catalyst is extremely similar to that of the Pt/C catalyst, and these MA values are almost double that of the PtNi/CNF catalyst. The PtNi/CNT and Pt/C catalysts, having similar MA values, suggest that both catalysts have similar current densities. Conversely, the SA values of the PtNi/CNT and PtNi/CNF catalysts are higher than that of commercial Pt/C catalysts. Since the SA value of the PtNi/CNT catalyst is higher than that of commercial Pt/C catalysts, the PtNi/CNT catalyst has a higher current density. Therefore, the PtNi/CNT catalyst electrokinetics supports our conviction that this material is suitable for use as a cathode electrode in PEMFCs.

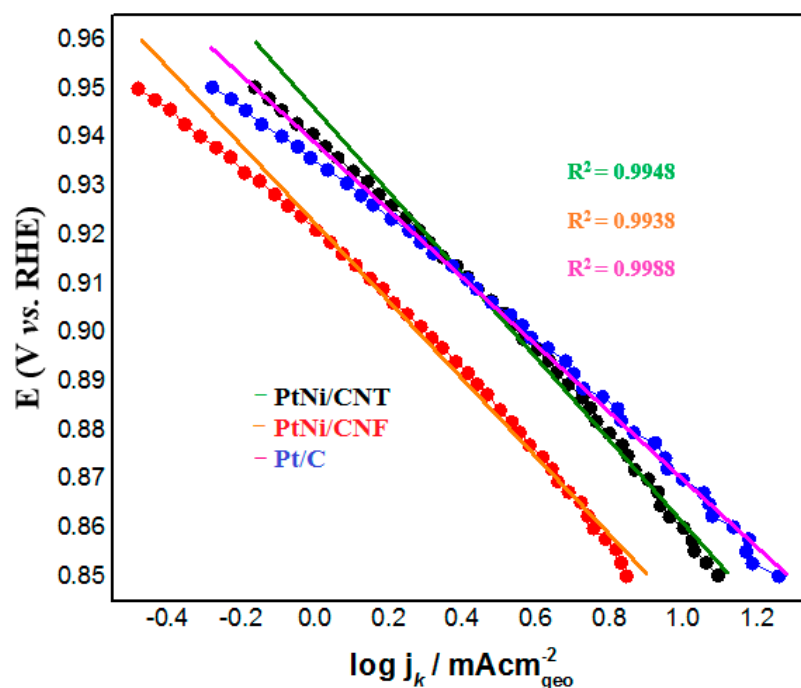


Figure 8. Tafel plots of PtNi/CNT, PtNi/CNF and Pt/C catalysts.

Figure 9 illustrates Koutecky–Levich plots deduced from hydrodynamic experiments, where the number of electrons transferred per oxygen molecule is determined. The PtNi/CNT and PtNi/CNF catalysts had  $B_0$  values of 0.1245 and 0.1263  $\text{mA cm}^{-2} \text{rpm}^{-1/2}$ , respectively, which agree with the  $B_0$  value of 0.1080  $\text{mA cm}^{-2} \text{rpm}^{-1/2}$  for the Pt/C catalyst calculated under the same experimental conditions. These results suggest that the ORR is governed by a four-electron and four-proton transfer pathway ( $n = 4e^-$ ) to water formation (i.e.,  $\text{O}_2 + 4\text{H}^+ + 4e^- \rightarrow 2\text{H}_2\text{O}$ ).

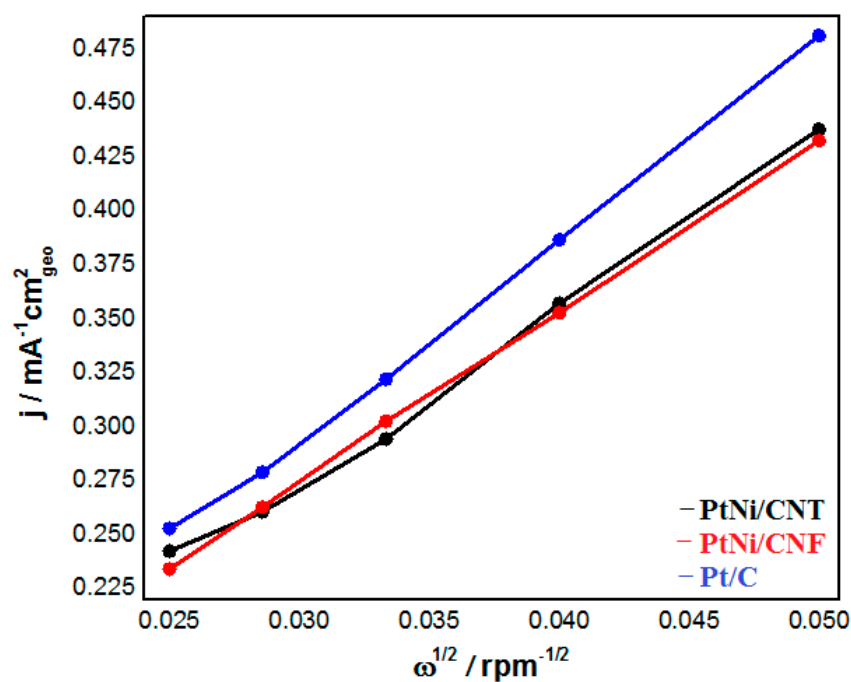


Figure 9. Koutecky–Levich plots of the PtNi/CNT, PtNi/CNF, and Pt/C catalysts at rotation rate of 1600 rpm.

Table 2 shows a comparison of the ORR activities of the PtNi/CNT catalysts and other Pt-based and Pt alloy-based electrocatalysts from the literature [25,31,49–52]. It can be seen that our PtNi/CNT catalyst performed competitively, particularly considering the simple synthesis used and the fact that the CNTs were used as a support material without any additional treatment. It is worth mentioning that the electrocatalysts in the literature were obtained via different processes and were supported on CNTs modified using different methods, such as heat treatment [49], hybrid support of CNTs and some type of metal oxide [50], hybrid structures between the catalyst and the CNT [25], one-step solvothermal method of PtNi/CNT [31], doping CNTs with some heteroatom [51], and partially exfoliating CNTs [52].

**Table 2.** Comparison of ORR activity of Pt and Pt alloys catalysts supported on CNT.

Catalyst	ECSA ( $\text{m}^2 \text{g}^{-1} \text{Pt}$ )	SA @ 0.9 V ( $\text{mA cm}^{-2} \text{Pt}$ )	MA @ 0.9 V ( $\text{A mg}^{-1} \text{Pt}$ )	Reference
PtNi/CNT	12.15	1.45	0.180	This work
Pt/MWCNT-RT <sup>a</sup>	Not given	0.26	0.017	[49]
Pt/MWCNT-300 <sup>b</sup>	Not given	0.32	0.020	[49]
Pt/MWCNT-400 <sup>b</sup>	Not given	0.29	0.006	[49]
Pt/MWCNT-500 <sup>b</sup>	Not given	0.15	0.007	[49]
Pt/MWCNT-600 <sup>b</sup>	Not given	0.15	0.007	[49]
Pt/MWCNT-700 <sup>b</sup>	Not given	0.15	0.003	[49]
Pt/TiO <sub>2</sub> @CNT	99.3	0.36	0.358	[50]
PtNi-MWCNT	47.9	1.07	0.510	[25]
PtNi/CNT	34.8	1.38	0.479	[31]
Pt <sub>3</sub> Co/N-CNT	565	0.09	0.050	[51]
Pt <sub>3</sub> Co/N-CNT <sub>HT</sub> <sup>c</sup>	34.9	0.06	0.019	[51]
Pt <sub>3</sub> Co/S-CNT	23.1	0.11	0.025	[51]
Pt <sub>3</sub> Ni/N-CNT	34.7	0.01	0.033	[51]
Pt <sub>3</sub> Ni/N-CNT <sub>HT</sub> <sup>c</sup>	46.4	0.06	0.029	[51]
Pt <sub>3</sub> Ni/S-CNT	5.6	0.14	0.001	[51]
Pt <sub>3</sub> Sc/PE <sup>d</sup> -CNT	102.1	Not given	0.080	[52]
Pt/PE <sup>d</sup> -CNT	95.7	Not given	0.070	[52]
Pt <sub>3</sub> Sc/CNT	62.4	Not given	0.060	[52]

<sup>a</sup> RT: room temperature, <sup>b</sup> (°C), <sup>c</sup> HT: heat treatment, <sup>d</sup> PE: partially exfoliated.

It is important to point out that the PtNi/CNT catalyst was obtained through a simple synthesis method that does not include additional steps involving additional reagents and/or energy; in turn, the CNTs and CNFs that served as supports were used as received, and no additional treatment was applied to them; so, this catalyst could be considered as an advantageous option to be used as cathodic catalysts for the ORR in PEMFC, since the PtNi/CNT electrocatalyst obtained in this work showed, in some cases, higher ECSA, MA, and SA than other Pt-Ni catalysts supported on modified CNT.

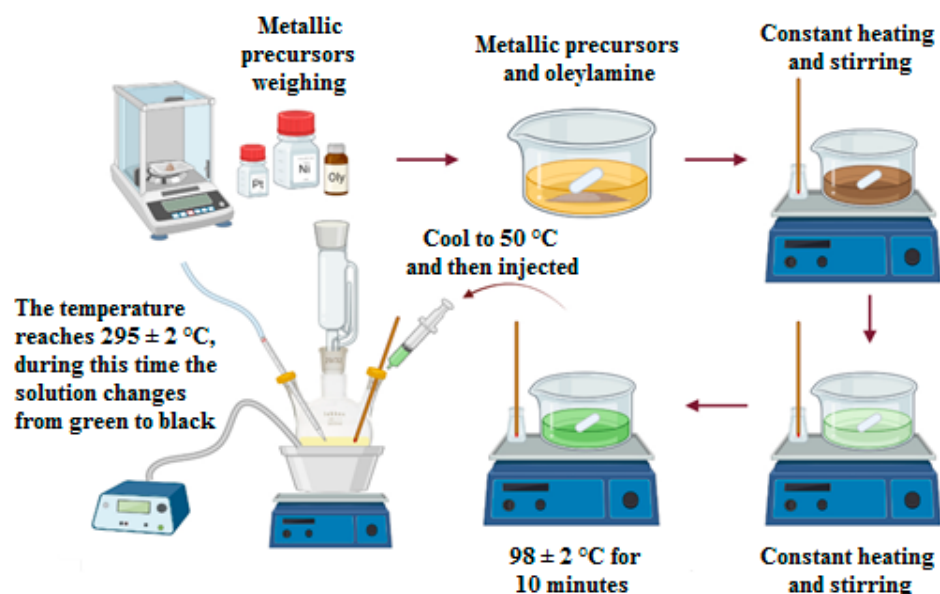
### 3. Materials and Methods

#### 3.1. Reagents

Oleylamine (>70%), hexachloroplatinic (IV) acid hexahydrate ( $\text{H}_2\text{PtCl}_6 \cdot 6\text{H}_2\text{O}$ ;  $\geq 37.50\%$  Pt), nickel (II) nitrate hexahydrate ( $\text{Ni}(\text{NO}_3)_2 \cdot 6\text{H}_2\text{O}$ ; 98%), CNTs, and CNFs were obtained from Sigma-Aldrich, St. Louis, MO, USA. All chemical reagents were used as received without further purification.

### 3.2. Synthesis of PtNi Alloy Nanoparticles

For the synthesis of PtNi nanoparticles, the metallic precursors Ni (NO<sub>3</sub>)<sub>2</sub>·6H<sub>2</sub>O (14.09 mg) and H<sub>2</sub>PtCl<sub>6</sub>·6H<sub>2</sub>O (22.4 mg) were dissolved in 1 mL of oleylamine in one vial. The resulting solution was heated at 98 ± 2 °C for 10 min with constant stirring. Independently, 9 mL of oleylamine was heated in a three-neck flask at 160 °C for 30 min with stirring and in a N<sub>2</sub> atmosphere. The metal precursor solution was allowed to cool to 50 °C before being injected into the flask containing oleylamine. After injecting the precursor solution, the reaction mixture was allowed to stabilize at 160 °C for 10 min. Subsequently, the temperature of the solution was gradually increased to 295 ± 2 °C (Scheme 1). During this time, the solution changed from green to black, indicating that nanoparticles were formed. The reaction was stopped 5 min after reaching 295 ± 2 °C. Afterward, the solution was cooled to 50 °C. Finally, the reaction product nanoparticles were washed several times with a hexane–ethanol mixture to eliminate any remaining organic synthesis residue.



**Scheme 1.** Schematic array of as-synthesized PtNi nanoparticles.

### 3.3. Preparation of PtNi/CNT and PtNi/CNF Catalysts

After obtaining the PtNi nanoparticles, we averaged the weight of five different syntheses ( $\bar{X} = 6.82$  mg) to obtain a catalyst loading of 20 wt. % of PtNi dispersed in 80 wt. % of support material (CNTs or CNFs). The as-synthesized PtNi nanoparticles were mixed with the CNTs or CNFs in a hexane–ethanol mixture (50:50 vol. %) under sonication for 1 h, resulting in a powder catalyst with a metal content of 20 wt. %. The PtNi catalyst was obtained by centrifugation at 5000 rpm for 10 min. The final powder catalysts were dried at 100 °C for 1 h under N<sub>2</sub> atmosphere. In addition, the CNTs and CNFs were used without being pre-treated.

### 3.4. Physical Characterization

XRD was used to analyze the crystalline structure of the PtNi nanoparticles. XRD was also used to identify the phases of the PtNi nanoparticles and was performed using a Bruker (BRUKER AXS, Inc., MA, USA) diffractometer at 25 ± 3 °C with Cu K- $\alpha$  radiation ( $\lambda = 1.54$  Å). The presented phases were identified using the International Center for Diffraction Data (ICDD) database ([https://www.icdd.com/?gclid=Cj0KCCQjwpImTBhCmARIsAKr58cyXZI4Tvmw7PZppw3grIue73MQsvMhGGKugz809Hhtb73DDdOAmEkwaAucWEALw\\_wcB](https://www.icdd.com/?gclid=Cj0KCCQjwpImTBhCmARIsAKr58cyXZI4Tvmw7PZppw3grIue73MQsvMhGGKugz809Hhtb73DDdOAmEkwaAucWEALw_wcB), accessed on 22 February 2021). Elemental analysis of the PtNi nanoparticles was performed using an EDS system adapted to a Zeiss Auriga scanning electron microscope (SEM;

Carl Zeiss, Oberkochen, Germany) under an acceleration voltage of 20 kV. The elemental analysis result was obtained by averaging the values of several zones of the catalyst surface. Finally, the morphology and particle size of the PtNi nanoparticles were determined using an ARM200F-JEOL microscope (JEOL, Tokyo, Japan) operated at 200 keV.

### 3.5. Electrochemical Measurements

Catalyst ink-type electrodes were prepared for the PtNi/CNT, PtNi/CNF, and commercial Pt/C catalysts (Pt/C Etek<sup>®</sup> 20 wt.%) with a Pt loading of  $20 \pm 2 \mu\text{g}_{\text{Pt}} \text{cm}^{-2}$  and deposited on a glassy-carbon disk to form a thin-film electrode ( $0.196 \text{ cm}^2$ ) [47]. Electrochemical measurements were performed using a three-electrode electrochemical cell. A platinum mesh was used as the counter electrode, and a reference hydrogen electrode (RHE) as the reference electrode. All the reported data were corrected by the uncompensated resistance in the cell. The electrochemical procedures were performed on a potentiostat/galvanostat (Metrohm Autolab B.V., Utrecht, Utrecht, The Netherlands). The catalytic activity of the samples was determined using CV, CO stripping, and RDE measurements. A detailed description of these techniques has been previously provided by our research group [7,46]. All measurements were conducted in a 0.1 M HClO<sub>4</sub> electrolyte solution.

## 4. Conclusions

The developed synthetic methodology (using oleylamine and hot injection of the metallic precursors) was efficient and reproducible in producing polyhedral homogeneous PtNi nanoparticles. Furthermore, it was demonstrated that the same techniques used for depositing Pt/C catalysts can be used to deposit PtNi nanoparticles on pristine supports (CNTs and CNFs). The presence of the PtNi alloy was confirmed using XRD. The TEM micrographs revealed polyhedral nanoparticles with an average size of 30 nm. The SEM micrographs confirmed the deposition of the PtNi nanoparticles on the CNTs and CNFs. The chemical compositions determined using EDS-SEM were  $74.33 \pm 2.07 \text{ wt.}\%$  Pt and  $25.62 \pm 2.1 \text{ wt.}\%$  Ni, which agree with the nominal compositions (75 wt.% Pt and 25 wt.% Ni). The electrochemical results demonstrated that the PtNi/CNT catalyst has a similar MA to commercial Pt/C catalysts, but a higher SA for the ORR in an acidic medium. Finally, the catalytic activity of the PtNi/CNT catalyst demonstrated that it could be used as cathodic catalysts in PEMFCs.

**Author Contributions:** Conceptualization, J.C.O.-H., M.M.T.-C., O.S.-F. and D.I.M.; formal analysis, J.C.O.-H., M.M.T.-C. and O.S.-F.; investigation, J.C.O.-H. and M.M.T.-C.; writing—original draft preparation, J.C.O.-H., M.M.T.-C. and O.S.-F.; writing—review and editing, J.C.O.-H., M.M.T.-C., O.S.-F. and D.I.M. All authors have read and agreed to the published version of the manuscript.

**Funding:** This research was funded by National Council for Science and Technology, CONACYT, under grant number FSE 245920.

**Acknowledgments:** Juan C. Ortiz-Herrera acknowledges National Council for Science and Technology, CONACYT for the doctoral scholarship. The authors thank Rafael Ibarra for the revision of the English language of this manuscript.

**Conflicts of Interest:** The authors declare no conflict of interest.

## References

1. Wu, J.; Yang, H. Platinum-based oxygen reduction electrocatalysts. *Acc. Chem. Res.* **2013**, *46*, 1848–1857. [[CrossRef](#)] [[PubMed](#)]
2. Cruz-Martínez, H.; Tellez-Cruz, M.M.; Guerrero-Gutiérrez, O.X.; Ramírez-Herrera, C.A.; Salinas-Juárez, M.G.; Velázquez-Orsorio, A.; Solorza-Feria, O. Mexican contributions for the improvement of electrocatalytic properties for the oxygen reduction reaction in PEM fuel cells. *Int. J. Hydrogen Energy* **2019**, *44*, 12477–12491. [[CrossRef](#)]
3. Cruz-Martínez, H.; Rojas-Chávez, H.; Matadamas-Ortiz, P.T.; Ortiz-Herrera, J.C.; López-Chávez, E.; Solorza-Feria, O.; Medina, D.I. Current progress of Pt-based ORR electrocatalysts for PEMFCs: An integrated view combining theory and experiment. *Mater. Today Phys.* **2021**, *19*, 100406. [[CrossRef](#)]
4. Wakabayashi, N.; Takeichi, M.; Uchida, H.; Watanabe, M. Temperature dependence of oxygen reduction activity at Pt–Fe, Pt–Co, and Pt–Ni alloy electrodes. *J. Phys. Chem. B* **2005**, *109*, 5836–5841. [[CrossRef](#)]

5. Cruz-Martínez, H.; Tellez-Cruz, M.M.; Rojas-Chávez, H.; Ramírez-Herrera, C.A.; Calaminici, P.; Solorza-Feria, O. NiPdPt trimetallic nanoparticles as efficient electrocatalysts towards the oxygen reduction reaction. *Int. J. Hydrogen Energy* **2019**, *44*, 12463–12469. [[CrossRef](#)]
6. Flores-Rojas, E.; Cruz-Martínez, H.; Tellez-Cruz, M.M.; Pérez-Robles, J.F.; Leyva-Ramírez, M.A.; Calaminici, P.; Solorza-Feria, O. Electrocatalysis of oxygen reduction on CoNi-decorated-Pt nanoparticles: A theoretical and experimental study. *Int. J. Hydrogen Energy* **2016**, *41*, 23301–23311. [[CrossRef](#)]
7. Flores-Rojas, E.; Cruz-Martínez, H.; Rojas-Chávez, H.; Tellez-Cruz, M.M.; Reyes-Rodríguez, J.L.; Cabañas-Moreno, J.G.; Calaminici, P.; Solorza-Feria, O. A combined DFT and experimental investigation of Pt-wrapped CoNi nanoparticles for the oxygen reduction reaction. *Electrocatalysis* **2018**, *9*, 662–672. [[CrossRef](#)]
8. Cui, C.; Gan, L.; Li, H.-H.; Yu, S.-H.; Heggen, M.; Strasser, P. Octahedral PtNi nanoparticle catalysts: Exceptional oxygen reduction activity by tuning the alloy particle surface composition. *Nano Lett.* **2012**, *12*, 5885–5889. [[CrossRef](#)]
9. Wu, J.; Gross, A.; Yang, H. Shape and composition-controlled platinum alloy nanocrystals using carbon monoxide as reducing agent. *Nano Lett.* **2011**, *11*, 798–802. [[CrossRef](#)]
10. Jayabal, S.; Saranya, G.; Geng, D.; Lin, L.-Y.; Meng, X. Insight into the correlation of Pt-support interactions with electrocatalytic activity and durability in fuel cells. *J. Mater. Chem. A* **2020**, *8*, 9420–9446. [[CrossRef](#)]
11. Gerber, I.C.; Serp, P. A theory/experience description of support effects in carbon-supported catalysts. *Chem. Rev.* **2019**, *120*, 1250–1349. [[CrossRef](#)] [[PubMed](#)]
12. Anwar, M.T.; Yan, X.; Asghar, M.R.; Husnain, N.; Shen, S.; Luo, L.; Zhang, J. Recent advances in hybrid support material for Pt-based electrocatalysts of proton exchange membrane fuel cells. *Int. J. Energy Res.* **2019**, *43*, 2694–2721. [[CrossRef](#)]
13. Samad, S.; Loh, K.S.; Wong, W.Y.; Lee, T.K.; Sunarso, J.; Chong, S.T.; Wan-Daud, W.R. Carbon and non-carbon support materials for platinum-based catalysts in fuel cells. *Int. J. Hydrogen Energy* **2018**, *43*, 7823–7854. [[CrossRef](#)]
14. Soni, S.K.; Thomas, B.; Kar, V.R. A comprehensive review on CNTs and CNT-reinforced composites: Syntheses, characteristics and applications. *Mat. Today Commun.* **2020**, *25*, 101546. [[CrossRef](#)]
15. Shao, Y.; Yin, G.; Zhang, J.; Gao, Y. Comparative investigation of the resistance to electrochemical oxidation of carbon black and carbon nanotubes in aqueous sulfuric acid solution. *Electrochim. Acta* **2006**, *51*, 5853–5857. [[CrossRef](#)]
16. Lin, Z.; Ji, L.; Krause, W.E.; Zhang, X. Synthesis and electrocatalysis of 1-aminopyrene-functionalized carbon nanofiber-supported platinum–ruthenium nanoparticles. *J. Power Sources* **2010**, *195*, 5520–5526. [[CrossRef](#)]
17. Sharma, S.; Pollet, B.G. Support materials for PEMFC and DMFC electrocatalysts—A review. *J. Power Sources* **2012**, *208*, 96–119. [[CrossRef](#)]
18. Hsin, Y.L.; Hwang, K.C.; Yeh, C.-T. Poly(vinylpyrrolidone)-modified graphite carbon nanofibers as promising supports for PtRu catalysts in direct methanol fuel cells. *J. Am. Chem. Soc.* **2007**, *129*, 9999–10010. [[CrossRef](#)]
19. Maiyalagan, T. Pt–Ru nanoparticles supported PAMAM dendrimer functionalized carbon nanofiber composite catalysts and their application to methanol oxidation. *J. Solid State Electrochem.* **2009**, *13*, 1561–1566. [[CrossRef](#)]
20. Matsumoto, T.; Komatsu, T.; Arai, K.; Yamazaki, T.; Kijima, M.; Shimizu, H.; Takasawa, Y.; Nakamura, J. Reduction of Pt usage in fuel cell electrocatalysts with carbon nanotube electrodes. *Chem. Commun.* **2004**, *7*, 840–841. [[CrossRef](#)]
21. Li, X.; Hsing, I.-M. The effect of the Pt deposition method and the support on Pt dispersion on carbon nanotubes. *Electrochim. Acta* **2006**, *51*, 5250–5258. [[CrossRef](#)]
22. Nagao, D.; Shimazaki, Y.; Saeki, S.; Kobayashi, Y.; Konno, M. Effect of ultrasonic irradiation on carbon-supported Pt–Ru nanoparticles prepared at high metal concentration. *Colloids Surf. A Physicochem. Eng. Asp.* **2007**, *302*, 623–627. [[CrossRef](#)]
23. Satishkumar, B.; Vogl, E.M.; Govindaraj, A.; Rao, C.N.R. The decoration of carbon nanotubes by metal nanoparticles. *J. Phys. D Appl. Phys.* **1996**, *29*, 3173. [[CrossRef](#)]
24. Asset, T.; Job, N.; Busby, Y.; Crisci, A.; Martin, V.; Stergiopoulos, V.; Bonaud, C.; Serov, A.; Atanassov, P.; Chattot, R.; et al. Porous hollow PtNi/C electrocatalysts: Carbon support considerations to meet performance and stability requirements. *ACS Catal.* **2018**, *8*, 893–903. [[CrossRef](#)]
25. Du, S.; Lu, Y.; Malladi, S.K.; Xu, Q.; Steinberger-Wilckens, R. A simple approach for PtNi–MWCNT hybrid nanostructures as high performance electrocatalysts for the oxygen reduction reaction. *J. Mater. Chem. A* **2014**, *2*, 692–698. [[CrossRef](#)]
26. Guo, D.-J.; Cui, S.-K.; Cheng, D.; Zhang, P.; Jiang, L.; Zhang, C.-C. One-pot synthesis of PtNi alloy nanoflowers supported on multi-walled carbon nanotubes with superior electrocatalytic activity for the oxygen reductio. *J. Power Sources* **2014**, *255*, 157–162. [[CrossRef](#)]
27. Litkohl, H.R.; Bahari, A.; Gatabi, M.P. Improved oxygen reduction reaction in PEMFCs by functionalized CNTs supported Pt–M (M=Fe, Ni, Fe–Ni) bi-and tri-metallic nanoparticles as efficient electrocatalyst. *Int. J. Hydrogen Energy* **2020**, *45*, 23543–23556. [[CrossRef](#)]
28. Qiao, L.; Liao, M.; Chen, S.; Wei, Z.; Zhang, S. Synthesis of Pt<sub>3</sub>Ni-based functionalized MWCNTs to enhance electrocatalysis for PEM fuel cells. *J. Solid State Electrochem.* **2014**, *18*, 1893–1898. [[CrossRef](#)]
29. Rosado, G.; Verde, Y.; Valenzuela-Muñoz, A.M.; Barbosa, R.; Yoshida, M.M.; Escobar, B. Catalytic activity of Pt–Ni nanoparticles supported on multi-walled carbon nanotubes for the oxygen reduction reaction. *Int. J. Hydrogen Energy* **2016**, *41*, 23260–23271. [[CrossRef](#)]
30. Wang, Y.; Li, G.; Jin, J.; Yang, S. Hollow porous carbon nanofibers as novel support for platinum-based oxygen reduction reaction electrocatalysts. *Int. J. Hydrogen Energy* **2017**, *42*, 5938–5947. [[CrossRef](#)]

31. Wang, J.; Li, B.; Yang, D.; Lv, H.; Zhang, C. Preparation of an octahedral PtNi/CNT catalyst and its application in high durability PEMFC cathodes. *RSC Adv.* **2018**, *8*, 18381–18387. [[CrossRef](#)]
32. Becknell, N.; Son, Y.; Kim, D.; Li, D.; Yu, Y.; Niu, Z.; Lei, T.; Sneed, B.T.; More, K.L.; Markovic, N.M.; et al. Control of architecture in rhombic dodecahedral Pt–Ni nanoframe electrocatalysts. *J. Am. Chem. Soc.* **2017**, *139*, 11678–11681. [[CrossRef](#)] [[PubMed](#)]
33. Chen, S.; Niu, Z.; Xie, C.; Gao, M.; Lai, M.; Li, M.; Yang, P. Effects of catalyst processing on the activity and stability of Pt–Ni nanoframe electrocatalysts. *ACS Nano* **2018**, *12*, 8697–8705. [[CrossRef](#)] [[PubMed](#)]
34. Reyes-Rodríguez, J.L.; Velázquez-Osorio, A.; Solorza-Feria, O.; Bahena-Urbe, D.; Roque, J. Influence of the injection temperature on the size of Ni–Pt polyhedral nanoparticles synthesized by the hot-injection method. *MRS Commun.* **2017**, *7*, 947–952. [[CrossRef](#)]
35. Mourdikoudis, S.; Liz-Marzán, L.M. Oleylamine in nanoparticle synthesis. *Chem. Mater.* **2013**, *25*, 1465–1476. [[CrossRef](#)]
36. Liu, Y.; Chen, H.; Tian, C.; Geng, D.; Wang, D.; Bai, S. One-Pot Synthesis of Highly Efficient Carbon-Supported Polyhedral Pt<sub>3</sub>Ni Alloy Nanoparticles for Oxygen Reduction Reaction. *Electrocatalysis* **2019**, *10*, 613–620. [[CrossRef](#)]
37. Wang, Y.-J.; Zhao, N.; Fang, B.; Li, H.; Bi, X.T.; Wang, H. Carbon-supported Pt-based alloy electrocatalysts for the oxygen reduction reaction in polymer electrolyte membrane fuel cells: Particle size, shape, and composition manipulation and their impact to activity. *Chem. Rev.* **2015**, *115*, 3433–3467. [[CrossRef](#)]
38. Antolini, E. Carbon supports for low-temperature fuel cell catalysts. *Appl. Catal. B Environ.* **2009**, *88*, 1–24. [[CrossRef](#)]
39. Choi, S.-I.; Xie, S.; Shao, M.; Lu, N.; Guerrero, S.; Odell, J.H.; Park, J.; Wang, J.; Kim, M.J.; Xia, Y. Controlling the size and composition of nanosized Pt–Ni octahedra to optimize their catalytic activities toward the oxygen reduction reaction. *ChemSusChem* **2014**, *7*, 1476–1483. [[CrossRef](#)]
40. Shao, M.; Chang, Q.; Dodelet, J.-P.; Chenitz, R. Recent advances in electrocatalysts for oxygen reduction reaction. *Chem. Rev.* **2016**, *116*, 3594–3657. [[CrossRef](#)]
41. Zhang, G.; Shao, Z.-G.; Lu, W.; Xie, F.; Xiao, H.; Qin, X.; Yi, B. Core–shell Pt modified Pd/C as an active and durable electrocatalyst for the oxygen reduction reaction in PEMFCs. *Appl. Catal. B Environ.* **2013**, 183–194. [[CrossRef](#)]
42. Huang, X.; Zhao, Z.; Cao, L.; Chen, Y.; Zhu, E.; Lin, Z.; Li, M.; Yan, A.; Zettl, A.; Wang, Y.M.; et al. High-performance transition metal-doped Pt<sub>3</sub>Ni octahedra for oxygen reduction reaction. *Science* **2015**, *348*, 1230–1234. [[CrossRef](#)] [[PubMed](#)]
43. Vidaković, T.; Christov, M.; Sundmacher, K. The use of CO stripping for in situ fuel cell catalyst characterization. *Electrochim. Acta* **2007**, *52*, 5606–5613. [[CrossRef](#)]
44. Mayrhofer, K.J.J.; Arenz, M.; Blizanac, B.B.; Stamenkovic, V.; Ross, P.; Markovic, N.M. CO surface electrochemistry on Pt-nanoparticles: A selective review. *Electrochim. Acta* **2005**, *50*, 5144–5154. [[CrossRef](#)]
45. Ciapina, E.G.; Santos, S.F.; Gonzalez, E.R. Electrochemical CO stripping on nanosized Pt surfaces in acid media: A review on the issue of peak multiplicity. *J. Electroanal. Chem.* **2018**, *815*, 47–60. [[CrossRef](#)]
46. Tellez-Cruz, M.M.; Padilla-Islas, M.A.; Godínez-Salomón, J.F.; Lartundo-Rojas, L.; Solorza-Feria, O. Y-OH-decorated-Pt/C electrocatalyst for oxygen reduction reaction. *Int. J. Hydrogen Energy* **2016**, *41*, 23318–23328. [[CrossRef](#)]
47. Garsany, Y.; Baturina, O.A.; Swider-Lyons, K.E.; Kocha, S.S. Experimental methods for quantifying the activity of platinum electrocatalysts for the oxygen reduction reaction. *Anal. Chem.* **2010**, *82*, 6321–6328. [[CrossRef](#)]
48. Alfaro-López, H.M.; Valdés-Madrigal, M.A.; Rojas-Chávez, H.; Cruz-Martínez, H.; Padilla-Islas, M.A.; Tellez-Cruz, M.M.; Solorza-Feria, O. A Trimetallic Pt<sub>2</sub>NiCo/C Electrocatalyst with Enhanced Activity and Durability for Oxygen Reduction Reaction. *Catalysts* **2020**, *10*, 170. [[CrossRef](#)]
49. Hussain, S.; Erikson, H.; Kongi, N.; Merisalu, M.; Ritslaid, P.; Sammelselg, V.; Tammeveski, K. Heat-treatment effects on the ORR activity of Pt nanoparticles deposited on multi-walled carbon nanotubes using magnetron sputtering technique. *Int. J. Hydrogen Energy* **2017**, *42*, 5958–5970. [[CrossRef](#)]
50. Kong, J.; Qin, Y.-H.; Wang, T.-L.; Wang, C.-W. Photodeposition of Pt nanoparticles onto TiO<sub>2</sub>@CNT as high-performance electrocatalyst for oxygen reduction reaction. *Int. J. Hydrogen Energy* **2020**, *45*, 1991–1997. [[CrossRef](#)]
51. Louisia, S.; Thomas, Y.R.J.; Lecante, P.; Heitzmann, M.; Axet, M.R.; Jacques, P.-A.; Serp, P. Alloyed Pt<sub>3</sub>M (M = Co, Ni) nanoparticles supported on S- and N-doped carbon nanotubes for the oxygen reduction reaction. *Beilstein J. Nanotechnol.* **2019**, *10*, 1251–1269. [[CrossRef](#)] [[PubMed](#)]
52. Garapati, M.S.; Sundara, R. Highly efficient and ORR active platinum-scandium alloy-partially exfoliated carbon nanotubes electrocatalyst for Proton Exchange Membrane Fuel Cell. *Int. J. Hydrogen Energy* **2019**, *44*, 10951–10963. [[CrossRef](#)]